crystals

MDPI

Article

Molecular Spectroscopic Imaging Offers a Systematic Assessment of Pathological Aortic Valve and Prosthesis Tissue in Biomineralization

Claudia Dittfeld [1,*], Alice Mieting [1], Cindy Welzel [1], Anett Jannasch [1], Klaus Matschke [1], Sems-Malte Tugtekin [1] and Gerald Steiner [2]

[1] Department of Cardiac Surgery, Carl Gustav Carus Faculty of Medicine, Technische Universität Dresden, Heart Centre Dresden, Fetscherstrasse 76, 01307 Dresden, Germany; alice.mieting@gmx.de (A.M.); cindy.welzel@tu-dresden.de (C.W.); anett.jannasch@tu-dresden.de (A.J.); Klaus.Matschke@herzzentrum-dresden.com (K.M.); Sems-Malte.Tugtekin@herzzentrum-dresden.com (S.-M.T.)

[2] Clinical Sensoring and Monitoring, Faculty of Medicine Carl Gustav Carus, Dresden University of Technology, 01307 Dresden, Germany; gerald.steiner@tu-dresden.de

* Correspondence: Claudia.Dittfeld1@tu-dresden.de

Received: 30 July 2020; Accepted: 26 August 2020; Published: 28 August 2020

Abstract: Pathological ECM remodelling and biomineralization in human aortic valve and bioprosthesis tissue were investigated by Fourier transformed infrared (FT-IR) spectroscopic imaging and multivariate data analysis. Results of histological von Kossa staining to monitor hydroxyapatite biomineralization correlated to the definition of mineralized tissue using FT-IR spectroscopic imaging. Spectra exhibit signals of carbonate and phosphate groups of hydroxyapatite. Proteins could be identified by the amide I and amide II bands. Proteins were detected in the calcified human aortic valve tissue, but no absorption signals of proteins were observed in the mineralized bioprosthesis sample region. A shift of the amide I band from 1654 cm^{-1} to 1636 cm^{-1} was assumed to result from β-sheet structures. This band shift was observed in regions where the mineralization process had been identified but also in non-mineralized bioprosthesis tissue independent of prior implantation. The increased occurrence of β-sheet conformation is hypothesized to be a promoter of the biomineralization process. FT-IR spectroscopic imaging offers a wealth of chemical information. For example, slight variations in band position and intensity allow investigation of heterogeneity across aortic valve tissue sections. The exact evaluation of these properties and correlation with conventional histological staining techniques give insights into aortic valve tissue remodelling and calcific pathogenesis.

Keywords: FT-IR spectroscopy; aortic valve tissue; biomineralization; bioprosthesis; PCA; von Kossa staining; histological correlation

1. Introduction

Aortic valve (AV) stenosis has a prevalence of more than 4.6 % in the population older than 75 [1,2]. This has social and economic relevance especially for the healthcare system. Fibrosis and calcific degeneration of AV tissue are the main pathological features leading to the need for surgical replacement of the AV leaflets by mechanical or preferentially biological prostheses [1,3]. On the one hand, mineralization is the result of changes in the extracellular matrix (ECM) by dystrophic intercalation, for example, after cell necrosis/apoptosis. On the other hand, it is said to result from an active cell-driven process in neoosteogenesis [1,3–7]. It has been proposed that the deterioration of biological AV prostheses 10 to 15 years after implantation results mainly from dystrophic acellular processes.

The reasons given for this include structural changes in the collagen protein due to pretreatment strategies, particularly fixation with glutaraldehyde [8–12].

Histological investigation of diseased human AV and prosthesis tissue but also of biological material under evaluation for the fabrication of biological prostheses such as bovine pericardium is often performed to monitor tissue structure and changes of the ECM [13]. However, the primary focus in prostheses material research is biomechanical testing accompanied by a biochemical evaluation of ECM composition [10,14]. These mostly degrading and destructive methods are time-consuming. In addition, they result in changes, for example, during experimental processing in histology [14]. Therefore, non-invasive spectroscopic approaches would be advantageous for investigating and characterizing mineralization and ECM structure. Spectral imaging of tissue sections of native diseased human AV tissue allows comparison to healthy tissue or to pericardial tissue processed for clinical use [14–18].

So far, Fourier transformed infrared (FT-IR) spectroscopy of human AV tissue has mainly been used to investigate hydroxyapatite (HAP) features without imaging tissue sections in larger two-dimensional areas [19–24]. Mineral AV deposits punctually analysed are composed of crystalline, amorphous inorganic calcium phosphates and low crystallinity biological hydroxyapatite [19–22,25]. Mangialardo et al. defined two types of substitutions by carbonate ions, the A type replacing OH^- and the B type replacing PO_4^{3-}. They can also occur together. The researchers suggested a formation mechanism in the human AV samples different from non-pathological mineralization processes in the body, because they detected carbonate substituted B-type HAP with lower crystallinity [21]. Alterations in mineral crystallinity are reflected by substantial alterations in the PO_4^{3-} contour, for example, after an increase of carbonate level [26]. B- and A-type substituted HAP also was detected by Delogne et al., using attenuated total reflection (ATR)-FT-IR analysis [27]. Dicalcium phosphate dehydrate (DCPD) and octacalcium phosphate (OCP) are precursor phases of the final stable salt HAP that results from DCPD and OCP by hydrolysis [22]. A higher DCPD and even more relevant OCP content has been ascribed to the biomineralization of porcine bioprostheses [22,28]. The punctual calculation of a Ca/P molar ratio is an alternative strategy to investigate the biomineralization of human AV and bioprostheses. It revealed values of 1.67 and 1.3, respectively, which are lower than in bone tissue (which was 2.2.) [28–30]. Taken together, biomineralic apatite can be described by the formula $(Ca,Na,Mg,X)_{10}(PO_4, HPO_4, CO_3)_6(OH,Y)_2$ in which X is the replacement of Ca by another cation, and Y can be chloride or fluoride, replacing OH depending on the individual tissue, the environment, and the pathological situation [25,29,31,32]. Chemical FT-IR imaging of native human AV tissue and mineralized explanted biological prosthesis material can be adapted to discover the heterogeneity of mineral deposits. Different pathological processes of dystrophic HAP intercalation and cell-driven processes such as neo-osteogenesis relevant in AV pathogenesis can be assigned to spectral properties [3,6,23,33,34]. Only one study describes FT-IR imaging of five different human AV tissues focussing HAP properties after defining the mineralized area using an area ratio of the phosphate vs. amide region [35]. The properties included crystallinity and the carbonate:phosphate ratio. Those authors concluded that crystallinity increased and carbonate content declined with increasing valve calcification status, and more mature minerals occur in later stages of AV biomineralization [35]. Raman imaging studies investigating human AV tissue focussed on both HAP and lipid features by blotting the integrated signal intensities of certain chemical characteristics that correlate to parallel histological sections in some studies [36–38].

However, the chemical definition of ECM composition and collagen conformation is of special relevance because changes in the protein matrix during fibrotic AV thickening or by treatment during prostheses fabrication may be causing this pathological biomineralization. The transition of the collagen conformation towards a higher β-sheet and random coil structure or changes in the collagen vs. elastin content are selectively monitored using FT-IR spectroscopy without imaging, and they are important aspects of the pathological in vivo AV situation [19,23,24,39]. Mechanical aspects can affect these IR spectroscopic characteristics. In porcine aortic valves, ATR-IR-spectroscopy revealed changes in the

amide I region after cyclic fatigue. This was interpreted to result from a loss of glycosaminoglycan (GAG) content [40]. In addition, changes in the composition of the extracellular matrix (e.g. collagen vs. elastin) can be quantified and chemically imaged by FT-IR spectroscopy accompanied by and in correlation to histological or biochemical (quantification) methods [14,41,42].

For the first time, human AV and xenogenous prosthesis tissue are presented in this FT-IR imaging study using cluster analysis and principal component analysis (PCA) to investigate tissue segments with the morphological characteristics of biomineralization. The aim was to define the methodological procedures and so the spectral parameters for systematic FT-IR spectroscopy of human AV and bioprostheses tissue. This was partially based on imaging and visualisation of chemical differences carved out by PCA. Besides the detailed analysis and verification of hydroxyapatite (e.g. crystalline and amorphous HAP), features of protein structure could be determined and extracted [14,19,41,43]. Both tissue characteristics can be clearly discriminated in the presented setup. The question whether IR-spectra of prosthesis samples carry information pointing to the future mineralization of tissue is addressed. FT-IR spectroscopy was preferred because the amide I vibration is very sensitive to the analysis of secondary structure, especially for the analysis of the α-helical vs. the β-sheet structure of collagen. Furthermore, the amide II band is weak or absent only in the Raman spectrum [44]. The presented datasets lead to the assumption that the protein structure of bovine pericardia in AV prostheses exhibits the same spectral properties as are found in mineralized tissue of human AV, but they differ from non-calcified human tissue.

In future studies, the molecular composition of a variety of samples can be analysed with FT-IR spectroscopy without the need for dyes or histological stains and independent of prior knowledge of the composition of the sample [33]. There will also be the potential for chemical imaging of larger tissue segments. The pathomechanisms of human AV and bioprostheses tissue—but also chemical properties after different steps in the pretreatment of xenogeneic pericardial patch/valve material for cardiac surgery—can be studied by FT-IR imaging using multiple samples.

2. Materials and Methods

2.1. Patient Material

Three calcified aortic valve tissues were used for the study after written informed consent was received from the patients. The study was approved by the ethics committee of the Dresden University (Ethikkomission an der TU Dresden, registration number EK429102015). The valves were replaced with prostheses during routine cardiac surgery. Two patients were male and one was female (average age 72.6 ± 1.2 years). All processed human AVs were tricuspid. Three explanted, calcified AV prosthesis tissues of different types all fabricated from bovine pericardium were investigated in the study: two Mitroflow valves (Sorin Group USA Inc, Arvada, CO, USA) and one Trifecta®aortic valve (St. Jude Medical, Inc.; St. Paul, MN, USA). As a control, tissue from a non-implanted prosthesis (Trifecta®) was analysed in parallel.

2.2. FT-IR Spectroscopy

AV or prosthesis tissues were embedded in cryosectioning media and frozen at −80 °C. Cryosections with a thickness of 5 µm were transferred to a CaF_2 window. FT-IR spectroscopic images were collected in transmission mode using an FT-IR spectrometer (Vertex 70) coupled with an infrared microscope (Hyperion 3000; both from Bruker Optik GmbH, Ettlingen, Germany) and nitrogen-cooled HgCdTe 64 × 64 focal plane array detector (Santa Barbara Focal Plane, Santa Barbara, CA, USA). The FPA is equipped with a Ge window which absorbs IR light below 950 cm^{-1}. The 15-fold Cassegrainian objective imaged a sample area of approx. 250 µm × 250 µm. Compositions of individual IR spectroscopic images of different samples were captured, subject to the size of the area investigated. Reference spectroscopic images were recorded from the pure calcium fluoride window before the tissue sections were investigated. For all measurements, a total of 100 interferograms (scans) were

co-added. The interferograms were Fourier transformed, applying Happ-Genzel apodization and a zero filling factor of 1. Spectra at a resolution of 6 cm^{-1} of the sample image were rationed against the spectra of the reference image and transferred to absorbance values. This spectral resolution was chosen to improve the signal-to-noise ratio, to reduce the size of the spectral data set, and to ensure that all prominent bands, even those with medium intensity, appeared clearly in the spectrum.

2.3. Data Preprocessing and Multivariate Analysis

The spectral data were evaluated using the Matlab Package (Version 7, Math Works Inc. Natick, MA, USA). Only the so-called fingerprint region between 950 cm^{-1} and 1800 cm^{-1} was considered. Data preprocessing involved only the removal of outliers. Outliers are spectra that are obviously not associated with soft tissue or mineralized tissue or spectra with a maximum absorbance value larger than 1.5. A baseline correction was not applied, since the exact form of the baseline was unknown and to avoid an uncontrolled loss of information. A k-means cluster analysis was carried out on the vector-normalized spectra by using the kmeans function of the Statistics Toolbox of Matlab. The squared Euclidean distance measure was chosen to minimize the distance between cluster members. Spectra in the range of 1480 cm^{-1} to 1730 cm^{-1} were analysed by principal component analysis (PCA). PCA was performed on the vector-normalized spectra of the raw matrix by using the eig function of the Statistics Toolbox of Matlab. The contrast of IR spectroscopic brightfield images was generated by integrating all absorbance values in the spectral range between 950 cm^{-1} and 1800 cm^{-1}.

2.4. Histological Staining

Tissue samples were embedded in cryomedium and cryosectioned with a thickness of 5 µm. Mineralization was visualised using von Kossa staining combined with HE according to standard methods. Staining was performed using parallel sections on glass slides or directly on CaF2 slides after IR spectroscopy. Images were acquired using a Slide Scanner (Axio ScanZ.1 by Zeiss, Jena, Germany) or Zeiss Observer Z.1.

3. Results

Mineralized human AV tissue was investigated by IR spectroscopic imaging. Regions to investigate were defined according to visible light evaluation at the border of a mineralized nodulus, but potentially non-mineralized tissue also was studied (Figure 1A,B).

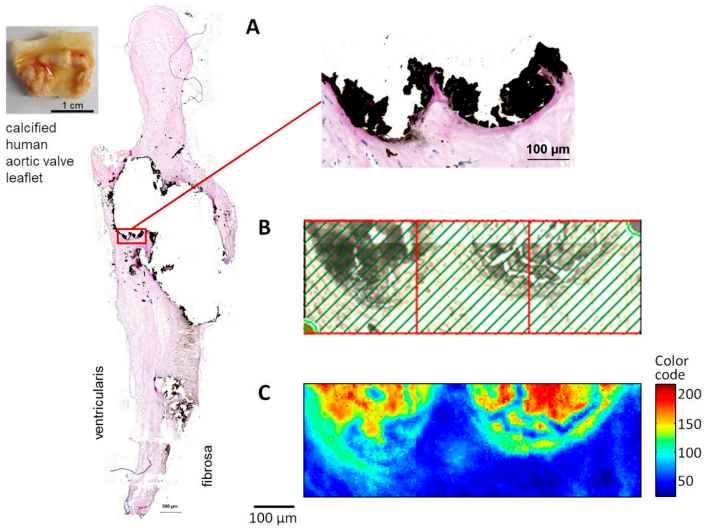

Figure 1. Von Kossa/HE staining of human AV sample with region analysed in FT-IR spectroscopic imaging.

(**A**) calcified human AV leaflet and resulting histological von Kossa/HE staining. The original aortic valve leaflet is shown on the left (fibrosa side) and the image with higher magnification is on the right. (**B**) resulting brightfield and (**C**) IR spectroscopic image of the region analysed by IR spectroscopic imaging.

Figure 1A shows a picture of the original AV leaflet (the fibrosa side, Figure 1A left) and the histological section of this leaflet stained with von Kossa combined with HE, which visualizes mineralization in black. A magnification of the part investigated in IR spectroscopy is shown. The section illustrates the complications that resulted from a sectioning technique of hydroxyapatite-bearing tissue without prior application of demineralization protocols. This material, which is poor in protein, tends to be sweep off the surface in the histological staining process. The typical structure of AV tissue is hardly preserved in the calcified human AV. The fibrosa layer exhibits mostly a high collagen content, and it is often the mineralization starting point. The section in Figure 1A shows that mineralization has spread through the entire leaflet to the ventricularis layer. The IR spectroscopic image is represented as a brightfield image in Figure 1C. The highest intensities (the red pixels) can be correlated to the mineralized tissue areas according to the von Kossa histological staining.

The mean (the bold line) and the standard deviation (grey area) are shown in Figure 2. Absorption bands of amide I (1600 cm^{-1}–1700 cm^{-1}) and amide II (1500 cm^{-1}–1600 cm^{-1}) dominate the spectral profile. Other, weaker absorption bands arise from CH groups of proteins and lipids located around 1400 cm^{-1} and 1460 cm^{-1}. The broad absorption band between 1000 cm^{-1} and 1150 cm^{-1} mainly originates from phosphate groups, carbohydrates and carbonate groups [45].

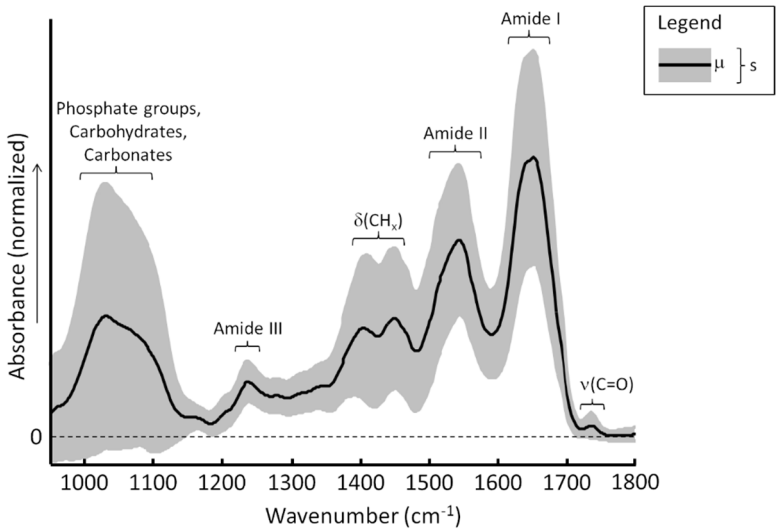

Figure 2. Mean FT-IR-spectrum (bold) and standard deviation (grey) calculated from the spectroscopic imaging data set of the human AV sample (see Figure 1). The most intense and prominent absorptions are assigned to proteins and to mineralized species.

To differentiate the components and mineralization status of certain tissue segments, and to evaluate the spectral features of a human AV section, a k-means cluster analysis was performed. The k-means cluster analysis is an often-used multivariate statistical method that examines the similarity between spectra. The cluster algorithm requires preselecting the number of clusters. This is often a critical decision since different numbers of clusters may lead to different results. It should be noted that the best or correct number of clusters is often unknown in advance. In spectroscopic data sets, however, the overlapping of clusters as well as noise and outliers are common. For this reason, the number of clusters was set at 10. Figure 3A–C shows the result of the k-means clustering of the calcified human AV leaflet.

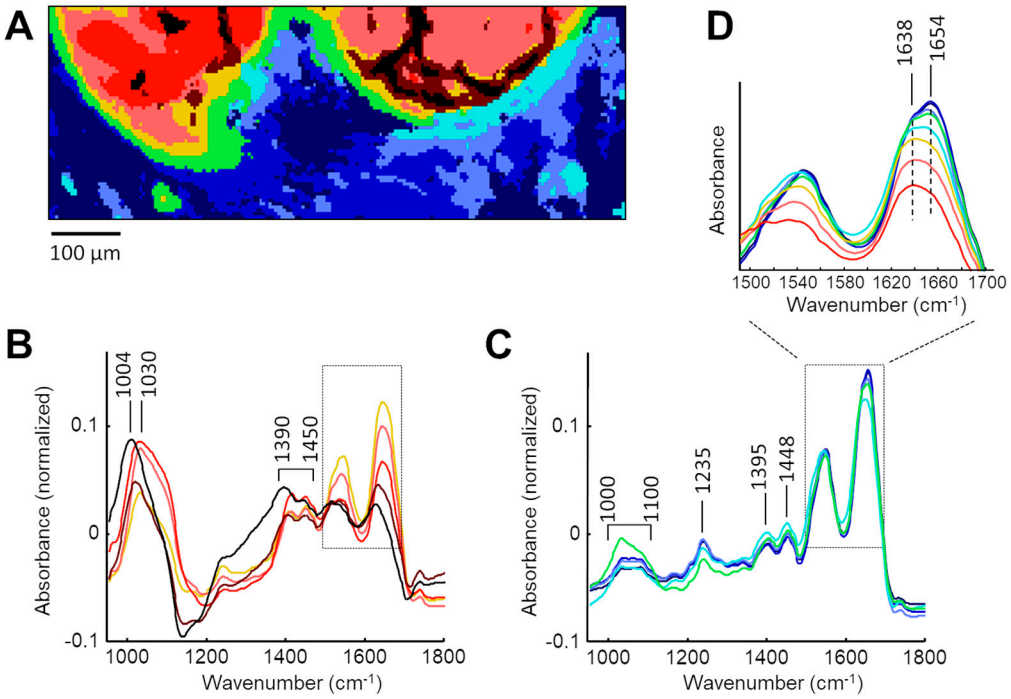

Figure 3. Results from k-means cluster analysis of the spectroscopic data set registrated from the calcified aortic valve leaflet (see Figure 1). (**A**) assignment of clusters. (**B**,**C**) corresponding cluster centroid spectra. (**D**) enlarged plot of selected centroid spectra in the region of amide I and amide II bands.

The algorithm sorted the clusters according to their similarity. While the highly mineralized sections were mainly represented by orange/reddish and brown pixels, blue and green pixels indicated a lower degree of mineralization. Centroid spectra of the mineralized regions are summarized in Figure 3B. The broad signal between 1000 cm^{-1} and 1100 cm^{-1} as well as bands around 1390 cm^{-1} and 1450 cm^{-1} can be assigned to phosphate groups of hydroxyapatite [46]. Two stronger signals between 1500 cm^{-1} and 1720 cm^{-1}, framed by the dotted rectangle, indicate the amide II and amide I bands, respectively [45]. The centroid spectra of brown and black clusters show a broad and strong absorption signal with a maximum at around 1004 cm^{-1}. This can be assigned to carbonate and phosphate groups [47]. The amide I and amide II bands appear only as weak features on a strong and broad background signal. Thus, the spectral absorption profiles of the black and brown clusters point to a high degree of mineralization and reduced content of proteins.

In contrast to Figure 3B, the centroid spectra plotted in Figure 3C show the typical absorption profile of soft tissue. Proteins are represented by the amide III band at 1235 cm^{-1} as well as by the amide II and amide I modes (see Figure 3D) [18]. Two weaker absorption bands at 1395 cm^{-1} and 1448 cm^{-1} are attributed to deformation modes of CH_x- groups [18]. The broad absorption signal between 1000 cm^{-1} and 1150 cm^{-1} was composed of many overlapping absorption bands among other things due to carbohydrates and phosphate groups of DNA. Only the green cluster indicates marginal mineralization by a slightly stronger absorption at 1030 cm^{-1}. Clearly, the infrared spectrum captured a wealth of chemical information and slight variations in the band positions, and intensities revealed heterogeneity across the tissue section. Although the centroid spectra that represent no or marginal mineralization are quite similar, the enlarged plots of the amide I and amide II regions (Figure 3D) show a shift of the amide I band maximum. The variation of the amide I spectral profile, especially of the maximum band position, indicates alterations in the secondary structure. Alpha helical structures show an absorption maximum at 1654 cm^{-1}. β-sheets exhibit a maximum band position at lower frequencies [18]. Therefore, we interpreted the shift of the amide I band from 1654 cm^{-1} to 1636 cm^{-1}

as an increase of β-sheet structures. More β-sheet was observed for regions where the mineralization process had been identified as advanced (orange and reddish pixels).

Calcified explanted bioprosthesis tissue that originated from bovine pericardium was studied in an equivalent examination strategy. Figure 4 shows the area stained by von Kossa combined with HE analysed by IR spectroscopic imaging of consecutive sections. Tissue mineralization is visualized in black (Figure 4A). The IR spectroscopic brightfield image is shown in Figure 4B. White pixels of the brightfield image in Figure 4C indicate spectra that were detected as outliers and removed.

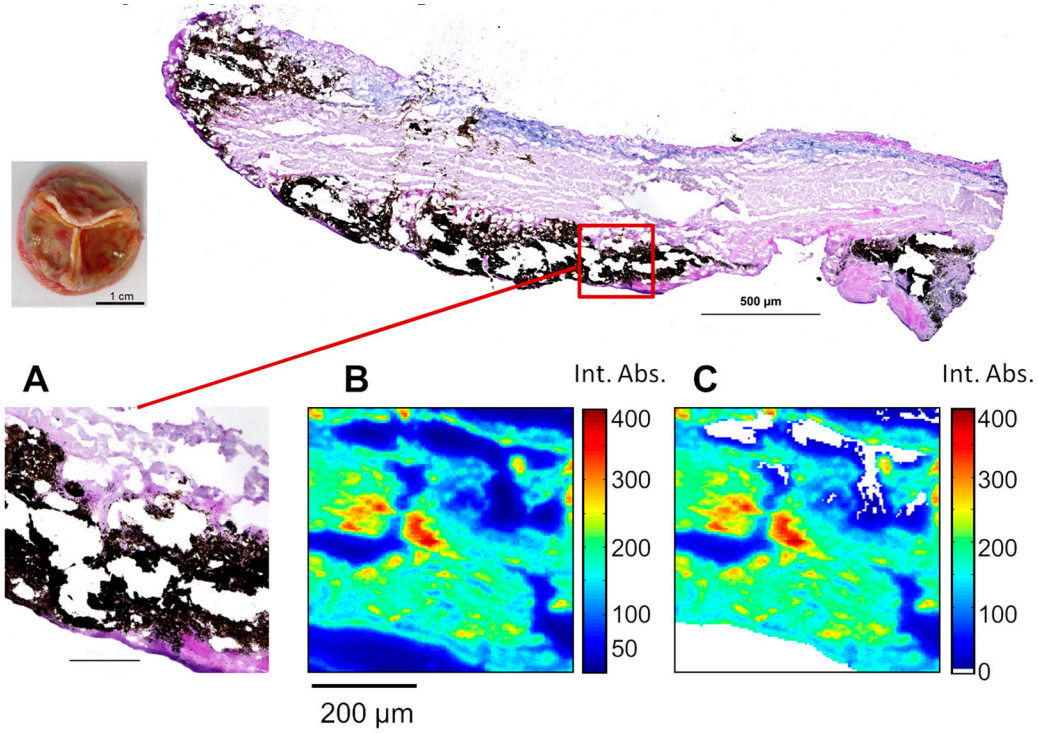

Figure 4. Von Kossa/HE staining of a calcified bioprosthesis sample with region analysed in FT-IR imaging. (**A**) calcified bioprosthesis sample and resulting histological von Kossa/HE staining" (entire section in the upper panel). (**B**) IR spectroscopic image (brightfield image) and (**C**) IR spectroscopic image after preprocessing. White pixels indicate outliers.

The cluster analysis of the calcified AV prosthesis sample is represented in Figure 5. Mineralized regions are represented by black, brown, reddish and orange pixels. The corresponding centroid spectra in Figure 5B are dominated by a broad absorption between 1000 cm^{-1} and 1150 cm^{-1}. A weaker signal at 1400 cm^{-1} is assigned to a stretching mode of carbonate groups [31]. The small absorption band at 1645 cm^{-1} might have come from bound water. However, the absorption signals of proteins (e.g. amide I and amide II bands) were not present. This indicates the total mineralization of the corresponding sample region. Figure 5C summarizes the centroid spectra of pixels with a certain content of proteins. In particular, the green cluster is characterized by strong mineralization, but the other centroid spectra also exhibit stronger signals in the region between 1000 cm^{-1} and 1150 cm^{-1} than the blue clusters in Figure 3. The absorption bands associated with CH_x - groups are located at 1382 cm^{-1} and 1443 cm^{-1}. Compared to Figure 3C, the maximum band positions are shifted to lower frequencies. This red-shift may indicate stronger intra-molecular interactions caused by the depositing of minerals. Figure 5D shows a general red-shift of the amide I bands. Three of the five centroid spectra show a maximum around 1638 cm^{-1}. The maximum of the other two centroid spectra shifted even more to 1626 cm^{-1}. The shifting of the amide I band and the variations of the profile of the amide II band clearly point to changes of the protein conformation.

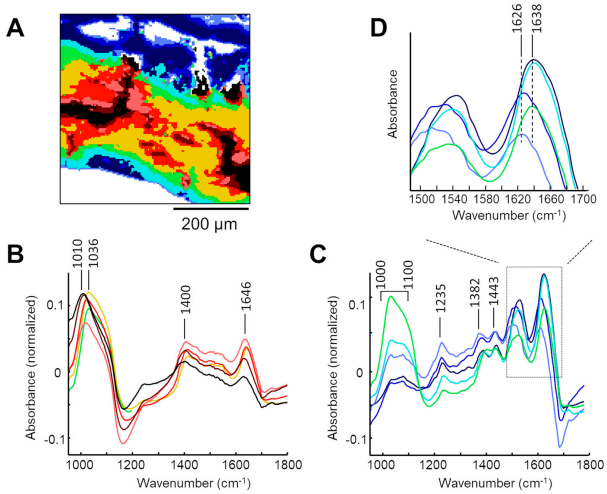

Figure 5. Results of k-means cluster analysis of the spectroscopic data set registered from the calcified AV prostheses (see Figure 4). (**A**) assignment of clusters. (**B**) corresponding cluster centroid spectra of the predominantly mineralized regions. (**C**) cluster centroid spectra of regions that contain a certain protein fraction. (**D**) enlarged plot in the region of amide I and amide II bands.

Similar to Figure 1; Figure 4, staining by von Kossa combined with HE was performed on consecutive sections of non-implanted bioprosthesis tissue of bovine pericardial origin (Figure 6A). No mineralization was detected. The selected FT-IR imaging region and the resulting intensity images are shown in Figure 6B–D.

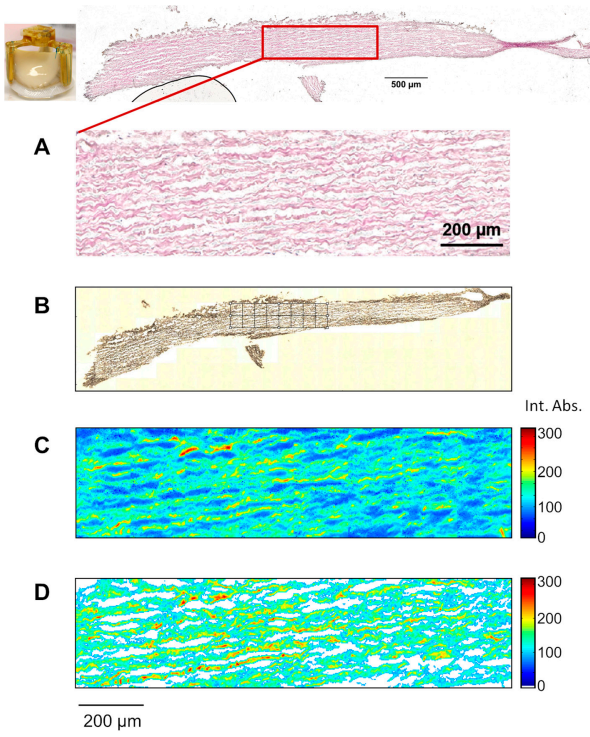

Figure 6. Von Kossa/HE staining of a non-implanted bioprosthesis sample with region analysed in FT-IR imaging. (**A**) bioprosthesis sample and resulting histological von Kossa/HE staining (entire section in the upper panel). (**B**) region analysed by IR spectroscopic imaging (**C**) IR spectroscopic image (brightfield image) and (**D**) IR spectroscopic image after preprocessing. White pixels indicate outliers.

Figure 7 shows the result of the k-means cluster analysis of the non-implanted prosthesis. The pattern of cluster assignment in Figure 7A shows substantial variances that must be accounted for in the prospect of characterizing the prosthesis. However, the centroid spectral profiles (Figure 7B) appear at first glance to be quite similar to one another. The spectra are dominated by the amide I band between 1600 cm^{-1} and 1700 cm^{-1} and the amide II band between 1500 cm^{-1} and 1580 cm^{-1}.

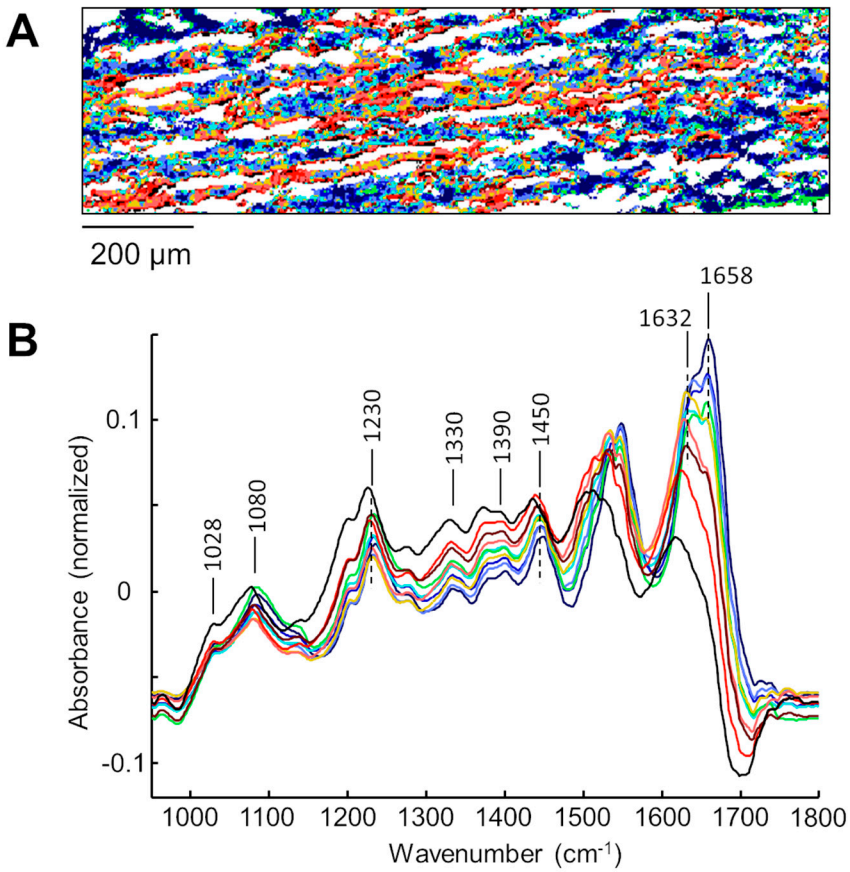

Figure 7. Results of k-means cluster analysis of the spectroscopic data set registrated from the non-implanted prosthesis sample. (**A**) assignment of clusters. (**B**) corresponding cluster centroid spectra.

Weaker protein absorptions include the amide III band at 1203 cm^{-1} and a number of peptide side-chain vibrations of CH_x- groups that occur at 1450 cm^{-1}, 1390 cm^{-1} and 1330 cm^{-1} [18]. The absorption bands at 1028 cm^{-1} and 1080 cm^{-1} are assigned to C-O groups. It must be noted that no absorption bands of mineralized tissue are observed. The maximum band position of the amide I band clearly shows two components at 1632 cm^{-1} and 1658 cm^{-1}. The absorption between 1600 cm^{-1} and 1700 cm^{-1} becomes progressively less intense as the maximum moves toward lower frequencies.

The key question addressed here is whether the structural information of the amide I band latent in these spectra is relevant to the mineralization of the prosthesis. Although the characteristic changes in protein structure and the accompanying mineralization processes can be observed through staining and visible examination, it is postulated that substantial variations occur on the molecular level before visible changes become apparent. For example, the formation and changes to the β-sheet associated with a lower content of α-helix structures can support the mineralization process. It is precisely these molecular changes that IR spectroscopy is suited to detect. Thus, there is great potential in the prospect of detecting conformation of the collagen matrix that show no visual abnormalities. The central aim of this exploratory proof of concept study is to determine whether IR spectra of prosthesis samples carry information pointing to the future mineralization of tissue.

To address this question, the variation of the amide I band was analysed by PCA. PCA provides a rapid way to assess variation within the spectral data set, and it assumes no explicit statistical model underlying the variance of the original spectra. Principal components (PC) are formed by loading plots and score images. The loading plots correspond to spectral bands where the variation is highest and weight the signals in the positive and negative direction. The score map reveals the weight of the loading plot for each pixel of the image. PCA is applied on the spectral range of the amide I band between 1580 cm^{-1} and 1730 cm^{-1}.

Only spectra that belong to a cluster that exhibits a clear profile of the amide I band were considered for PCA. So, the spectra of the calcified aortic valve leaflet, the calcified AV prosthesis and the non-implanted prosthesis were composed into one large data set on which PCA was performed. The reassembled score images and the loading vectors of the three PC's are represented in Figures 8 and 9, respectively.

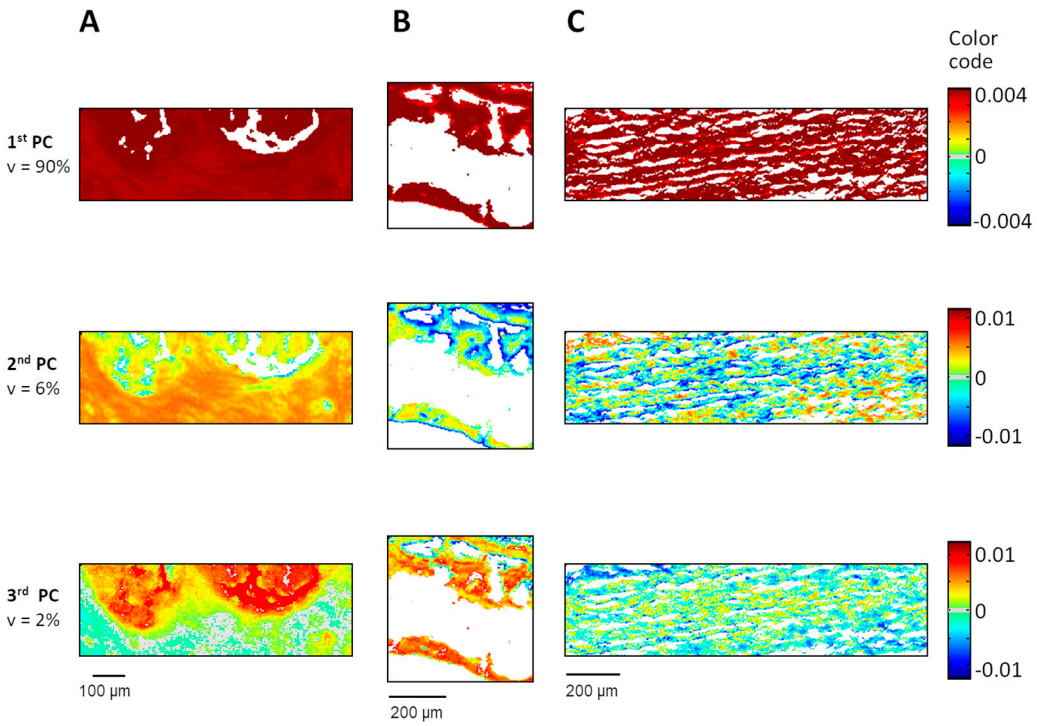

Figure 8. Results of PCA of the spectroscopic data set showing score images of (**A**) mineralized aortic valve leaflet, (**B**) mineralized AV prosthesis and (**C**) non-implanted prosthesis. Score images are printed in the rainbow colour code where blue colours represent low values and red colours high values. Gray pixels indicate a score value of zero, and white pixels represent spectra that were not involved in PCA. The percentage values display the amount of variance covered by the particular PC.

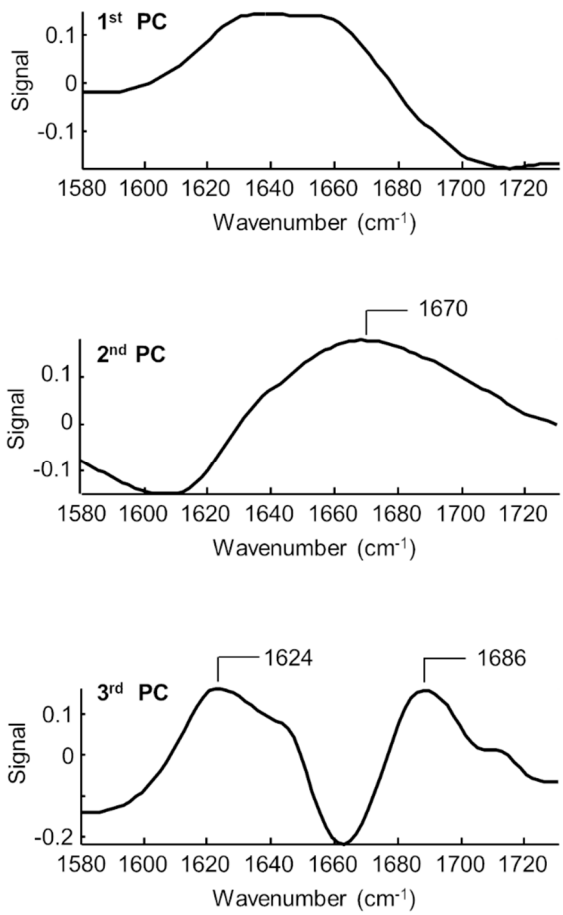

Figure 9. Loading plots of the first three PC's of the PCA of the mineralized aortic valve leaflet, the mineralized AV prosthesis and the non-implanted prosthesis.

The 1st PC exhibits a variance of 90%. It represents the mean spectrum of the samples. The amide I band appears as a broad signal (Figure 8). All score images of the 1st PC are dominated by dark red/brown pixels, and they confirm the presence of proteins. The score images of the 2nd PC show clear differences between the samples. The corresponding loading plot displays a positive signal with a maximum at 1670 cm^{-1}. This frequency is attributed to anti-parallel β-sheet structures. Chartreuse and yellow pixels dominate the score map of the calcified aortic valve leaflet (Figure 8A), and they indicate only slight variations. In contrast to them, score values of calcified AV prostheses (Figure 8B) and the non-implanted prosthesis (Figure 8C) show distinct variations across the image. The score images of the 3rd PC show large variations for all samples. Red pixels of the calcified aortic valve leaflet (Figure 8A) correspond very well with mineralized regions of the sample. This characteristic is also supported by the score map of the calcified AV prosthesis (Figure 8B). The non-implanted prosthesis (Figure 8C) shows a certain number of red and orange pixels, although this sample is not mineralized. The loading plot of the 3rd PC has positive signals at 1624 cm^{-1} and 1686 cm^{-1}. The first signal arises from the parallel β-sheet. Unsorted random coils and turns contribute to the signal around 1680 cm^{-1}. An increased occurrence of β-sheet structures is hypothesized as a promoter of the mineralization process. Higher PC's predominantly represent noise signals without any further relevant information.

4. Discussion

Various aspects of AV research can be investigated using FT-IR spectroscopy to cover basic science and materials research but also in vitro substance testing analyses [14,19–24,35,48]. Pathological human AV tissue niches with different environmental compositions can exhibit diverse types of apatite and

precursors as well as changes in ECM matrix composition and conformation [49]. The correlation of certain spectroscopic parameters in fingerprint regions for characteristics of apatite and/or amide protein characteristics with pathological mechanisms of dystrophic mineralization or osteogenesis is the aim of ongoing research. This demands the histological evaluation of human AV sections in parallel to FT-IR spectroscopy and the definition of chemical properties according to ECM niches and calcified nodule morphology comparable to bone tissue evaluation [50]. In turn, the detailed knowledge of ECM characteristics in mineralized AV tissue—but also in regions with fibrotic ECM remodelling—is important for material research. The longevity of xenogeneic prosthesis tissue such as bovine pericardium can be improved. Aspects of collagen protein conformation but also changes in ECM composition such as the reduction of glycosaminoglycans or the fragmentation of elastin fibres are relevant and can be examined with FT-IR imaging.

Investigation of ECM characteristics and biomineralization in human aortic valve tissue and in bioprosthetic pericardial tissue using FT-IR imaging in correlation with histological routine staining techniques is presented herein. The absorption bands of amide I and amide II, as well as the bands arising from CH-groups of proteins and lipids and from phosphate groups, carbohydrates and carbonate groups are ascribed. The hydroxyapatite biomineralization features (wavenumber 1000 cm^{-1}–1150 cm^{-1}) in FT-IR-spectroscopic images correspond to the histological definition of mineralization in von Kossa staining. PCA of amide I allows the detailed chemical investigation and resulting imaging of multiple samples. It allows the evaluation of pathophysiological situations in a single sample as well as between-group comparisons. Changes in the secondary protein structure can be monitored in addition to the biomineralization [44].

Three biomineralized human AV samples and bioprostheses derived from bovine pericardium were investigated. There was an increase of β-sheet conformation at 1624 cm^{-1} in mineralized human AV tissue and in mineralized regions of bioprosthesis pericardial tissue, but it also occurred in the absence of bioprosthesis mineralization. To support the observation, a non-implanted bioprosthesis tissue was examined, and the higher β-sheet signal was confirmed in that tissue. An increased occurrence of β-sheet is therefore hypothesized as a promoter of the mineralization process. Reasons for this higher content of β-sheet conformation are still to be determined. The ECM structure of bovine pericardium differs from human AV tissue. The three-layered healthy aortic valve comprises fibrosa, spongiosa and the ventricularis layer with different predominant ECM components such as collagen (fibrosa), glycosaminoglycans (spongiosa) and elastin (ventricularis) [51,52]. In diseased AV tissue, the original three-layered structure is hardly assignable, and a fibrotic ECM enrichment can be observed. The protein expression pattern is dysregulated [53]. Therefore, the evaluation of the samples in FT-IR-imaging in this study was performed without being classified to a certain layer of the valve.

Pericardial tissue used for bioprostheses fabrication is homogenous, without the layered structure seen in human AV. It consists mainly of collagen, glycosaminoglycans and elastin, and it differs from the ECM composition in human AV [54–56]. Tissue mineralization can be determined by the natural content of certain ECM molecules but also by the conformation of protein, especially after preparation strategies such as glutaraldehyde fixation.

New strategies are being developed to prepare bovine pericardium, for example, without the use of glutaraldehyde but with intense decellularization of the tissue to remove antigens that can induce an immune response after transplantation. These strategies can be accompanied by and evaluated by FT-IR spectroscopy [14]. This allows chemical monitoring of the matrix in addition to but without the need for time-consuming, degrading and destructive methods, since methods and parameters to evaluate spectroscopic data are defined. Analysis of in vitro mineralization of patch material in bioreactors with incubation in solutions that reflect body fluids can not only be performed regarding protein conformation and composition but also to monitor the biomineralization process and the chemical apatite type [22,27,28,57]. In the future, bioreactors or microfluidic devices can therefore even feature IR spectroscopy as an endoscopic technology to monitor the mineralization process of incubated materials, for example, under pulsatile fluid conditions in situ.

There are great advantages and a wide spectrum of research questions and material that can be investigated by FT-IR spectroscopy in AV research. However, numerous challenges are yet to be resolved. In this setup, three human AV tissues and three mineralized bioprostheses were analysed, and comparable results were obtained. Therefore, the results of one representative sample are shown. Preparation of the tissue for FT-IR imaging, in this case, was performed without decalcification. Calcified AV tissue can hardly be cryosectioned. For chemical imaging of highly calcified human AV tissue, a decalcifying protocol like the one used in bone research must be adopted for sample preparation, or an alternative embedding procedure must be used [6,35,50,58,59]. Decalcifying pretreatment using acid or EDTA solutions can influence FT-IR spectroscopy signals. The possibility of comparing these data with specimens that have not undergone that procedure is yet to be proven. As an alternative or in addition, attenuated total reflection (ATR)-IR-spectroscopy of AV tissue samples (and also surfaces) can enhance the sample spectrum in the research field [14,60]. The most important challenge for the data analysis is the correlation of the changes in wavenumbers of FT-IR spectroscopy signals with pathology-related chemical variations in apatite and ECM properties. The chemical imaging can be associated with histological analyses such as staining of parallel sections with von Kossa combined with HE, alizarin red dye or Movat Pentachrom staining for defining neoosteogenesis for example [6].

Furthermore, FT-IR imaging results of biomineralization in human AV tissue are important for classifying in vitro mineralization protocols using human valvular interstitial cells. Mineralic deposits in these cultures are often visualized using alizarin red staining, but this is under critical discussion [61–63]. The differentiation of these cells to a myofibroblast but also osteogenic type of cells contribute to AV sclerosis and is focus of AV research [61]. Validation of the exact mineral composition in the in vitro setups is an important aspect to reflect their applicability, for example, for substance testing [48,64,65].

This study reports on the use of IR spectroscopy for the characterization and classification of mineralized human AV and bioprosthesis tissues. To our knowledge, this is the first time that biomineralized tissue of human aortic valve and bioprosthesis tissue have been studied by IR spectroscopic imaging. The IR spectrum provides a very high degree of structural information, and it reflects the amounts of various classes of molecules and other species. Moreover, the sensitivity of IR spectroscopy—especially IR spectroscopic imaging—extends to the finer variations within the tissue. The combination of IR spectroscopic imaging with multivariate spectral feature extraction has clear potential in medicine, and a growing body of literature suggests molecular spectroscopy as a diagnostic tool.

5. Conclusions

The multivariate evaluation of spectral datasets using cluster and principal component analysis presented herein offers a comprehensive analytical tool to examine ECM composition or protein conformation. Compared to histological von Kossa staining, using FT-IR spectroscopy apatitic mineralization is clearly distinguishable from non-mineralized tissue in a chemical map. In human AV mineralization, this was co-detected with amide characteristics, whereas in the bioprosthesis mineralization amid bands was seen only in the border with non-mineralized tissue. Wavenumbers reflecting a shift towards β-sheet protein conformation were detected in calcified human AV tissue, in both non-mineralized and mineralized bioprosthetic sections, and in an original bioprosthesis tissue of bovine pericardial origin. These observations have now to be investigated in several additional samples and according to bioprosthesis tissue pretreatment. Using a higher resolution for FT-IR spectroscopic imaging, the chemical composition of apatitic material can be mapped and correlated to pathological features. The aim of ongoing strategies is to be able to analyse and map exact apatitic composition and changes in protein conformation and correlate that information with pathophysiological features such as osteogenesis or dystrophic calcification.

Author Contributions: Conceptualization, C.D., A.M. and G.S.; methodology, C.D., A.M., C.W., G.S.; validation, C.D., A.J. and G.S.; investigation, A.M., C.D., G.S.; resources, K.M., G.S.; data curation, G.S.; writing—original draft preparation, C.D., G.S.; writing—review and editing, S.-M.T.; supervision, K.M., S.-M.T., G.S.; All authors have read and agreed to the published version of the manuscript.

Funding: The research received no external funding. Open Access is funded by the Publication Fund of the TU Dresden.

Acknowledgments: The excellent technical assistance of Maria Feilmeier and Dominic Salminger is acknowledged. Histological images were acquired and processed using equipment of the Biopolis Dresden Imaging Platform at the BIOTEC/CRTD–Light Microscopy Facility and the MTZ-Core Facility Cellular Imaging.

Conflicts of Interest: The authors declare no conflict of interest.

References

1. Rajput, F.A.; Zeltser, R. Aortic Valve Replacement. In *StatPearls*; StatPearls Publishing: Treasure Island, FL, USA, 2019.
2. Coffey, S.; Cairns, B.J.; Iung, B. The modern epidemiology of heart valve disease. *Heart* **2016**, *102*, 75–85. [CrossRef] [PubMed]
3. Hutcheson, J.D.; Goettsch, C.; Rogers, M.A.; Aikawa, E. Revisiting cardiovascular calcification: A multifaceted disease requiring a multidisciplinary approach. *Semin. Cell. Dev. Biol.* **2015**, *46*, 68–77. [CrossRef] [PubMed]
4. Kunitake, J.A.M.R.; Choi, S.; Nguyen, K.X.; Lee, M.M.; He, F.; Sudilovsky, D.; Morris, P.G.; Jochelson, M.S.; Hudis, C.A.; Muller, D.A.; et al. Correlative imaging reveals physiochemical heterogeneity of microcalcifications in human breast carcinomas. *J. Struct. Biol.* **2018**, *202*, 25–34. [CrossRef]
5. Mohler, E.R., 3rd; Gannon, F.; Reynolds, C.; Zimmerman, R.; Keane, M.G.; Kaplan, F.S. Bone formation and inflammation in cardiac valves. *Circulation* **2001**, *103*, 1522–1528. [CrossRef]
6. Dittfeld, C.; Haase, M.; Feilmeier, M.; Jannasch, A.; Buttner, P.; Plotze, K.; Waldow, T.; Tugtekin, S.M. Movat Pentachrom stain reveals unexpected high osteogenesis rate in aortic valves. *Acta Histochem.* **2017**, *119*, 533–537. [CrossRef]
7. Rajamannan, N.M.; Subramaniam, M.; Rickard, D.; Stock, S.R.; Donovan, J.; Springett, M.; Orszulak, T.; Fullerton, D.A.; Tajik, A.J.; Bonow, R.O.; et al. Human aortic valve calcification is associated with an osteoblast phenotype. *Circulation* **2003**, *107*, 2181–2184. [CrossRef]
8. Fiedler, A.G.; Tolis, G., Jr. Surgical Treatment of Valvular Heart Disease: Overview of Mechanical and Tissue Prostheses, Advantages, Disadvantages, and Implications for Clinical Use. *Curr. Treat. Options Cardiovasc. Med.* **2018**, *20*, 7. [CrossRef]
9. Dvir, D.; Bourguignon, T.; Otto, C.M.; Hahn, R.T.; Rosenhek, R.; Webb, J.G.; Treede, H.; Sarano, M.E.; Feldman, T.; Wijeysundera, H.C.; et al. Standardized Definition of Structural Valve Degeneration for Surgical and Transcatheter Bioprosthetic Aortic Valves. *Circulation* **2018**, *137*, 388–399. [CrossRef]
10. Iop, L.; Palmosi, T.; Dal Sasso, E.; Gerosa, G. Bioengineered tissue solutions for repair, correction and reconstruction in cardiovascular surgery. *J. Thorac. Dis.* **2018**, *10*, S2390–S2411. [CrossRef]
11. Ma, B.; Wang, X.; Wu, C.; Chang, J. Crosslinking strategies for preparation of extracellular matrix-derived cardiovascular scaffolds. *Regen. Biomater.* **2014**, *1*, 81–89. [CrossRef]
12. Schoen, F.J.; Tsao, J.W.; Levy, R.J. Calcification of bovine pericardium used in cardiac valve bioprostheses. Implications for the mechanisms of bioprosthetic tissue mineralization. *Am. J. Pathol.* **1986**, *123*, 134–145. [PubMed]
13. Gomez-Stallons, M.V.; Tretter, J.T.; Hassel, K.; Gonzalez-Ramos, O.; Amofa, D.; Ollberding, N.J.; Mazur, W.; Choo, J.K.; Smith, J.M.; Kereiakes, D.J.; et al. Calcification and extracellular matrix dysregulation in human postmortem and surgical aortic valves. *Heart* **2019**, *105*, 1616–1621. [CrossRef]
14. Vasquez-Rivera, A.; Oldenhof, H.; Hilfiker, A.; Wolkers, W.F. Spectral fingerprinting of decellularized heart valve scaffolds. *Spectrochim. Acta A Mol. Biomol. Spectrosc.* **2019**, *214*, 95–102. [CrossRef]
15. Bunaciu, A.A.; Hoang, V.D.; Aboul-Enein, H.Y. Vibrational Micro-Spectroscopy of Human Tissues Analysis: Review. *Crit. Rev. Anal. Chem.* **2017**, *47*, 194–203. [CrossRef] [PubMed]
16. Krafft, C.P.J. Vibrational Spectroscopic Imaging of Soft Tissue. In *Infrared and Raman Spectroscopic Imaging*, 2nd ed.; Reiner Salzer, H.S., Ed.; Wiley: New York, NY, USA, 2014; pp. 113–152.

17. Byrne, H.J.; Baranska, M.; Puppels, G.J.; Stone, N.; Wood, B.; Gough, K.M.; Lasch, P.; Heraud, P.; Sule-Suso, J.; Sockalingum, G.D. Spectropathology for the next generation: Quo vadis? *Analyst* **2015**, *140*, 2066–2073. [CrossRef] [PubMed]
18. Movasaghi, Z.; Rehman, S.; Rehman, I.U. Fourier transform infrared (FTIR) spectroscopy of biological tissues. *Appl. Spectrosc. Rev.* **2008**, *43*, 134–179. [CrossRef]
19. Dritsa, V.; Pissaridi, K.; Koutoulakis, E.; Mamarelis, I.; Kotoulas, C.; Anastassopoulou, J. An infrared spectroscopic study of aortic valve. A possible mechanism of calcification and the role of magnesium salts. *In Vivo* **2014**, *28*, 91–98. [PubMed]
20. Prieto, R.M.; Gomila, I.; Costa-Bauza, A.; Bonnin, O.; Grases, F. Study on the structure and composition of aortic valve calcific deposits: Etiological aspects. *J. Biophys. Chem.* **2011**, *2*, 19–25. [CrossRef]
21. Mangialardo, S.; Cottignoli, V.; Cavarretta, E.; Salvador, L.; Postorino, P.; Maras, A. Pathological biominerals: Raman and infrared studies of bioapatite deposits in human heart valves. *Appl. Spectrosc.* **2012**, *66*, 1121–1127. [CrossRef]
22. Mikroulis, D.; Mavrilas, D.; Kapolos, J.; Koutsoukos, P.G.; Lolas, C. Physicochemical and microscopical study of calcific deposits from natural and bioprosthetic heart valves. Comparison and implications for mineralization mechanism. *J. Mater. Sci Mater. Med.* **2002**, *13*, 885–889. [CrossRef]
23. Anastassopoulou, J.; Kyriakidou, M.; Kyriazis, S.; Mavrogenis, A.F.; Mamareli, V.; Mamarelis, I.; Petra, M.; Malesiou, E.; Kotoulas, C.; Kolovou, P.; et al. Oxidative stress in ageing and disease development studied by FT-IR spectroscopy. *Mech. Ageing Dev.* **2018**, *172*, 107–114. [CrossRef] [PubMed]
24. Mamarelis, I.; Koutoulakis, E.; Kotoulas, C.; Dritsa, V.; Mamareli, V.; Anastassopoulou, J. FT-IR spectroscopic study of amyloid protein formation and aortic valve calcification. *Hell. J. Cardiol.* **2017**, *58*, 148–150. [CrossRef] [PubMed]
25. LeGeros, R.Z. Formation and transformation of calcium phosphates: Relevance to vascular calcification. *Z. Kardiol.* **2001**, *90*, 116–124. [CrossRef] [PubMed]
26. Ou-Yang, H.; Paschalis, E.P.; Mayo, W.E.; Boskey, A.L.; Mendelsohn, R. Infrared microscopic imaging of bone: Spatial distribution of CO3(2-). *J. Bone Miner. Res.* **2001**, *16*, 893–900. [CrossRef]
27. Delogne, C.; Lawford, P.V.; Habesch, S.M.; Carolan, V.A. Characterization of the calcification of cardiac valve bioprostheses by environmental scanning electron microscopy and vibrational spectroscopy. *J. Microsc.* **2007**, *228*, 62–77. [CrossRef]
28. Tomazic, B.B.; Brown, W.E.; Schoen, F.J. Physicochemical properties of calcific deposits isolated from porcine bioprosthetic heart valves removed from patients following 2−13 years function. *J. Biomed. Mater. Res.* **1994**, *28*, 35–47. [CrossRef]
29. Dorozhkin, S.V. Calcium orthophosphates: Occurrence, properties, biomineralization, pathological calcification and biomimetic applications. *Biomatter* **2011**, *1*, 121–164. [CrossRef]
30. Tsolaki, E.; Bertazzo, S. Pathological Mineralization: The Potential of Mineralomics. *Materials* **2019**, *12*, 3126. [CrossRef]
31. Boskey, A.; Mendelsohn, R. Infrared analysis of bone in health and disease. *J. Biomed. Opt.* **2005**, *10*, 031102. [CrossRef]
32. Rey, C.; Combes, C.; Drouet, C.; Glimcher, M.J. Bone mineral: Update on chemical composition and structure. *Osteoporos. Int.* **2009**, *20*, 1013–1021. [CrossRef]
33. Bhargava, R.; Madabhushi, A. Emerging Themes in Image Informatics and Molecular Analysis for Digital Pathology. *Annu. Rev. Biomed. Eng.* **2016**, *18*, 387–412. [CrossRef] [PubMed]
34. Boskey, A.; Pleshko Camacho, N. FT-IR imaging of native and tissue-engineered bone and cartilage. *Biomaterials* **2007**, *28*, 2465–2478. [CrossRef] [PubMed]
35. Richards, J.M.; Kunitake, J.; Hunt, H.B.; Wnorowski, A.N.; Lin, D.W.; Boskey, A.L.; Donnelly, E.; Estroff, L.A.; Butcher, J.T. Crystallinity of hydroxyapatite drives myofibroblastic activation and calcification in aortic valves. *Acta Biomater.* **2018**, *71*, 24–36. [CrossRef] [PubMed]
36. Bonetti, A.; Bonifacio, A.; Della Mora, A.; Livi, U.; Marchini, M.; Ortolani, F. Carotenoids co-localize with hydroxyapatite, cholesterol, and other lipids in calcified stenotic aortic valves. Ex vivo Raman maps compared to histological patterns. *Eur. J. Histochem.* **2015**, *59*, 2505. [CrossRef]
37. Czamara, K.; Natorska, J.; Kapusta, P.; Baranska, M.; Kaczor, A. Raman microspectroscopy of human aortic valves: Investigation of the local and global biochemical changes associated with calcification in aortic stenosis. *Analyst* **2015**, *140*, 2164–2170. [CrossRef]

38. Pilarczyk, M.; Czamara, K.; Baranska, M.; Natorska, J.; Kapusta, P.; Undas, A.; Kaczor, A. Calcification of aortic human valves studied in situ by Raman microimaging: Following mineralization from small grains to big deposits. *J. Raman. Spectrosc.* **2013**, *44*, 1222–1229. [CrossRef]
39. Jastrzebska, M.; Zalewska-Rejdak, J.; Mroz, I.; Barwinski, B.; Wrzalik, R.; Kocot, A.; Nozynski, J. Atomic force microscopy and FT-IR spectroscopy investigations of human heart valves. *Gen. Physiol. Biophys.* **2006**, *25*, 231–244.
40. Vyavahare, N.; Ogle, M.; Schoen, F.J.; Zand, R.; Gloeckner, D.C.; Sacks, M.; Levy, R.J. Mechanisms of bioprosthetic heart valve failure: Fatigue causes collagen denaturation and glycosaminoglycan loss. *J. Biomed. Mater. Res.* **1999**, *46*, 44–50. [CrossRef]
41. Bonnier, F.; Rubin, S.; Venteo, L.; Krishna, C.M.; Pluot, M.; Baehrel, B.; Manfait, M.; Sockalingum, G.D. In-vitro analysis of normal and aneurismal human ascending aortic tissues using FT-IR microspectroscopy. *Biochim. Biophys. Acta* **2006**, *1758*, 968–973. [CrossRef]
42. Belbachir, K.; Noreen, R.; Gouspillou, G.; Petibois, C. Collagen types analysis and differentiation by FTIR spectroscopy. *Anal. Bioanal. Chem.* **2009**, *395*, 829–837. [CrossRef]
43. Von Euw, S.; Wang, Y.; Laurent, G.; Drouet, C.; Babonneau, F.; Nassif, N.; Azais, T. Bone mineral: New insights into its chemical composition. *Sci. Rep.* **2019**, *9*, 8456. [CrossRef] [PubMed]
44. Barth, A. Infrared spectroscopy of proteins. *Biochim. Biophys. Acta* **2007**, *1767*, 1073–1101. [CrossRef] [PubMed]
45. Socrates, G. *Infrared and Raman Characteristic Group Frequencies*; Wiley: New York, NY, USA, 2001.
46. Paschalis, E.P.; Gamsjaeger, S.; Klaushofer, K. Vibrational spectroscopic techniques to assess bone quality. *Osteoporos. Int.* **2017**, *28*, 2275–2291. [CrossRef] [PubMed]
47. Lopes, C.D.A.; Limirio, P.H.J.O.; Novais, V.R.; Dechichi, P. Fourier transform infrared spectroscopy (FTIR) application chemical characterization of enamel, dentin and bone. *Appl. Spectrosc. Rev.* **2018**, *53*, 747–769. [CrossRef]
48. Dittfeld, C.; Reimann, G.; Mieting, A.; Buttner, P.; Jannasch, A.; Plotze, K.; Steiner, G.; Tugtekin, S.M.; Matschke, K. Treatment with XAV-939 prevents in vitro calcification of human valvular interstitial cells. *PLoS ONE* **2018**, *13*, e0208774. [CrossRef]
49. Cottignoli, V.; Relucenti, M.; Agrosi, G.; Cavarretta, E.; Familiari, G.; Salvador, L.; Maras, A. Biological Niches within Human Calcified Aortic Valves: Towards Understanding of the Pathological Biomineralization Process. *Biomed. Res. Int.* **2015**, *2015*, 542687. [CrossRef]
50. Khanarian, N.T.; Boushell, M.K.; Spalazzi, J.P.; Pleshko, N.; Boskey, A.L.; Lu, H.H. FTIR-I compositional mapping of the cartilage-to-bone interface as a function of tissue region and age. *J. Bone Miner. Res.* **2014**, *29*, 2643–2652. [CrossRef]
51. Leopold, J.A. Cellular mechanisms of aortic valve calcification. *Circ. Cardiovasc. Interv.* **2012**, *5*, 605–614. [CrossRef]
52. Schoen, F.J. Evolving concepts of cardiac valve dynamics: The continuum of development, functional structure, pathobiology, and tissue engineering. *Circulation* **2008**, *118*, 1864–1880. [CrossRef]
53. Schlotter, F.; Halu, A.; Goto, S.; Blaser, M.C.; Body, S.C.; Lee, L.H.; Higashi, H.; DeLaughter, D.M.; Hutcheson, J.D.; Vyas, P.; et al. Spatiotemporal Multi-Omics Mapping Generates a Molecular Atlas of the Aortic Valve and Reveals Networks Driving Disease. *Circulation* **2018**, *138*, 377–393. [CrossRef]
54. Dupont, S.; Morsut, L.; Aragona, M.; Enzo, E.; Giulitti, S.; Cordenonsi, M.; Zanconato, F.; Le Digabel, J.; Forcato, M.; Bicciato, S.; et al. Role of YAP/TAZ in mechanotransduction. *Nature* **2011**, *474*, 179–183. [CrossRef] [PubMed]
55. Li, N.; Li, Y.; Gong, D.; Xia, C.; Liu, X.; Xu, Z. Efficient decellularization for bovine pericardium with extracellular matrix preservation and good biocompatibility. *Interact. Cardiovasc. Thorac. Surg.* **2018**, *26*, 768–776. [CrossRef] [PubMed]
56. Braga-Vilela, A.S.; Pimentel, E.R.; Marangoni, S.; Toyama, M.H.; de Campos Vidal, B. Extracellular matrix of porcine pericardium: Biochemistry and collagen architecture. *J. Membr. Biol.* **2008**, *221*, 15–25. [CrossRef] [PubMed]
57. Pleshko, N.; Boskey, A.; Mendelsohn, R. Novel infrared spectroscopic method for the determination of crystallinity of hydroxyapatite minerals. *Biophys. J.* **1991**, *60*, 786–793. [CrossRef]

58. Abrantes, A.A.; Rafacho, A.; Rivero, E.R.; Mariano, F.V.; Siqueira, F.M.; Gondak, R.O. Tissue integrity, costs and time associated with different agents for histological bone preparation. *Microsc. Res. Tech.* **2017**, *80*, 344–349. [CrossRef]
59. Bogoevski, K.; Woloszyk, A.; Blackwood, K.; Woodruff, M.A.; Glatt, V. Tissue Morphology and Antigenicity in Mouse and Rat Tibia: Comparing 12 Different Decalcification Conditions. *J. Histochem. Cytochem.* **2019**, *67*, 545–561. [CrossRef]
60. Chan, K.L.A.; Kazarian, S.G. Attenuated total reflection Fourier-transform infrared (ATR-FTIR) imaging of tissues and live cells. *Chem. Soc. Rev.* **2016**, *45*, 1850–1864. [CrossRef]
61. Bogdanova, M.; Zabirnyk, A.; Malashicheva, A.; Enayati, K.Z.; Karlsen, T.A.; Kaljusto, M.L.; Kvitting, J.P.; Dissen, E.; Sullivan, G.J.; Kostareva, A.; et al. Interstitial cells in calcified aortic valves have reduced differentiation potential and stem cell-like properties. *Sci. Rep.* **2019**, *9*, 12934. [CrossRef]
62. Goto, S.; Rogers, M.A.; Blaser, M.C.; Higashi, H.; Lee, L.H.; Schlotter, F.; Body, S.C.; Aikawa, M.; Singh, S.A.; Aikawa, E. Standardization of Human Calcific Aortic Valve Disease in vitro Modeling Reveals Passage-Dependent Calcification. *Front. Cardiovasc. Med.* **2019**, *6*, 49. [CrossRef]
63. Cloyd, K.L.; El-Hamamsy, I.; Boonrungsiman, S.; Hedegaard, M.; Gentleman, E.; Sarathchandra, P.; Colazzo, F.; Gentleman, M.M.; Yacoub, M.H.; Chester, A.H.; et al. Characterization of porcine aortic valvular interstitial cell 'calcified' nodules. *PLoS ONE* **2012**, *7*, e48154. [CrossRef]
64. Hutcheson, J.D.; Aikawa, E.; Merryman, W.D. Potential drug targets for calcific aortic valve disease. *Nat. Rev. Cardiol.* **2014**, *11*, 218–231. [CrossRef] [PubMed]
65. Myasoedova, V.A.; Ravani, A.L.; Frigerio, B.; Valerio, V.; Moschetta, D.; Songia, P.; Poggio, P. Novel pharmacological targets for calcific aortic valve disease: Prevention and treatments. *Pharmacol. Res.* **2018**, *136*, 74–82. [CrossRef] [PubMed]